July – August 2020
ISSN: 0193-4120 Page No. 36 - 55

An Experimental Analysis and Modeling Approach of Response Surface Methodology to Predict the Mass Loss of HVOF Sprayed Coatings

[1]Daniel C. Ribu*, [2]R.Rajesh, [3]D.Thirumalaikumarasamy, and [5]R.Paventhan

[1]Daniel C. Ribu
Assistant Professor,
Department of Mechanical Engineering,
Lourdes Matha College of Science and Technology,
Thiruvananthapuram – 608 002,
Kerala,INDIA.
Email: ribucdaniel@gmail.com
Tel: +91-09995453358 (Mobile)

[2]R.Rajesh
Professor and Principal
Department of Mechanical Engineering,
Rohini College of Engineering & Technology,
Anjugramam– 629401,
Tamil Nadu,INDIA.
Email: rajesh1576@yahoo.co.in
Tel: +91-09894434131
Fax: +91-4652-266605

[3]D.Thirumalaikumarasamy
(Corresponding Author)*
Assistant Professor,
Department of Mechanical Engineering,
Government College of Engineering,
Bargur– 635104,Krishnagiri.
Tamil Nadu,INDIA.
Email: tkumarasamy412@gmail.com
Tel: +91-09894319865(Mobile)
Fax: +91-4144-238080/238275

[4] R.Paventhan
Professor
Department of Mechanical Engineering,
Er.Perumal Manimekalai College of Engineering,
Krishnagiri- 635117.Tamil Nadu,INDIA.
Email: mr_paventhan@yahoo.com
Tel: +91-09944013323(Mobile)

Article Info
Volume 83
Page Number: 36 - 55
Publication Issue:
July - August 2020

Abstract
The primary failure ways of the hydraulic turbine components, mud pumps and drill pipes are slurry erosion. The cermet coatings produced by HVOF spray method extensively utilized for enhance the slurry erosion performance of the materials. WC-12Co powders were coated on the 35CrMo steel through HVOF were studied in this research. Coatings structures were tested with SEM and XRD techniques, further microhardness, porosity and roughness were estimated. Moreover, the experiments were performed to explore the influence of rotational speed, angle of impingement, slurry concentration and time on the slurry erosion behaviour of the coatings. Empirical relationships were established to estimate the mass loss of coatings through response surface methodology. Four factors five level central composite rotatable design matrix was utilized to reduce the level of experimental conditions. The relationship established can be adequately utilized to estimate the

TEST Engineering & Management

July – August 2020
ISSN: 0193-4120 Page No. 36 - 55

Article History
***Article Received**: 06 June 2020*
***Revised**: 29 June 2020*
***Accepted**: 14 July 2020*
***Publication**: 25 July 2020*

mass loss of coatings at a confidence level of 95%. The rotational speed was the predominant parameter influencing the mass loss of the coatings followed by angle of impingement, slurry concentration and time.
Keywords: Slurry erosion; WC-12Co; HVOF; RSM;

Abbreviations:
HVOF: High velocity oxy fuel
HVAF: High velocity air fuel
SE: Slurry erosion
RSM: Response surface methodology
XRD: Xray diffraction

1.0 Introduction

In the field of ships, hydroelectric power plants, drilling and other industries, there is widespread erosion, which is a typical method of failure in present industrial machinery [1–2]. The erosion can be categorized into four groups according to the fluid medium,: cavitation erosion, sand-blasting erosion, slurry erosion and droplet erosion [3, 4].

For irrigation purposes submersible pumps are extensively used in Northern India [5]. The main essential parts of these submersible pumps are impellers and casings. During their operation, these impellers were more sensitive to the slurry erosion (SE) as they are exposed to the slurry (water mixed with sand particles). Owing to slurry erosion, not only does solid surface material receive plowed but it can also cause a bulk failure. [6]. The cavity bore submersible pumps are selected among the various classifications of submersible pumps as a result of the superior water quality they provide. In addition , in the case of cavity bore submersible pump, the slurry erosion has been revealed to be more severe due to the presence of greater amounts of better sand particles in water. The periodic impellers substitution produces a consequential economic loss to the group of farmers', twice a year. Likewise, due to slurry erosion problem, in hydraulic turbines of hydro power plants, parts like guide vanes, top and bottom ring liners, labyrinths, runner blades, and inlet valve seals further affected [7]. As the slurry erosion regularly appears on the machinery surface, hard coating preparation on its surface is an valuable approach to minimize the erosive particles destruction [8].

Stainless steel is a generally utilized material for these components which are exposed to slurry erosion conditions during extended disclosure is eroded, and its functionality is lost. Slurry erosion relies on the erodent particles shape and hardness. In slurry erosion, the conditions like angle of impingement, impact angle, rotational speed and time also perform a vital role, except the erodent particles shape and hardness [9]. To minimize the slurry erosion, numerous authors have attempted various classifications of coating methods and compositions of the coating to deposit these fluid machinery components. The traditional and bimodal coatings are known due to high hardness to increase the slurry erosion resistance compared to the uncoated substrate. The primary erosion mechanism in all the experimental conditions is the spalling of the coating, induced through crack development and dissemination during fatigue stress [10]. Compared to the bulk metal alloys, HVAF sprayed coatings express major performance enhancement in cavitation, slurry erosion and dry erosion wear circumstances [11]. The erosion wear improved at a non-linear level with an improved in the period of experiments, rotational speed of spindle and sand slurry concentration [12]. Compared with CoNiCrAlY coating all the conditions of slurry erosion, HVOF sprayed WC-Co-Cr coating show the improved erosion performance [13]. The micro structural refinement of friction stir processed Ni-Cr-Al2O3 coating was established through high velocity flame spray process [14]. The post-processed coating was attained with the enhanced hardness and fracture toughness. Owing to the hard phases of chromium carbide and nickel carbide, three times greater hardness of coatings was achieved, which limited the abrasive wear compared to uncoated steel. Furthermore, it was

July – August 2020
ISSN: 0193-4120 Page No. 36 - 55

noted that the erosion rate was higher, which would be stable after the surface became smooth and visible for longer periods [15].

According to the literature [10-15], it can be noted that a few research has been revealed on the erosion behavior of thermal sprayed coatings. However, it is therefore a reality that erosion resistance of a specific combination of substrate/coating relies on not only the characteristics of coating material although the properties of the substrate material. Moreover, this has been stated that there is limited or no data on the effect of slurry erosion variables on the erosion behavior of thermal sprayed coatings deposited on steel substrate. In the present study, conventional feedstock powder WC-10Co has been coated through the HVOF technique on a 35CrMo steel. The slurry jet erosion behavior of coatings was studied using a slurry erosion setup and the coating behavior was compared under the influence of four different variables: angle of impingement, rotational speeds, impact angle and time.

2. Experimental

In this study, WC-10Co powders were coated on a 35CrMo steel with the coating thickness of about 200 μm by HVOF (HIPOJET-2700, Make: Metallizing Equipment Co. Jodhpur, India) facility located at Annamalai University, India. Afterwards each and every run conditions the coating thickness were determined using digital micrometer (with an accuracy of 0.001mm). Coating thickness was attained by varying the number of deposition passes using 1, 2 and 3 passes. Photograph of HVOF spray machine and the coated specimens were shown in Fig.1. The substrate was preheated prior to coating: this has been achieved through one entire torch cycle at a pass velocity of 0.8 m/s, attaining a temperature of 120–180°C. The size of the specimens used in this investigation are 15 mm × 10 mm × 8 mm, whose sides had a chamfer with 1 mm of length and an angle 45°. These samples were washed in acetone through ultrasonic cleaning equipment. The surface roughness of the substrate was enhanced using corundum, grit size of 320 ± 500 μm. A surface roughness tester (Make: Mitutoyo, Japan; Model: Surf test 301) was utilized to estimate the roughness and after grit blasting the average roughness of the substrate was measured at 5-10 μm. The composition of the coating powders, which were manufactured from Metallizing Equipment Co, is as listed: WC-90 wt-% and Co-10 wt-%. The powder size of the particles is 15-45μm. Table 1 discloses the process variables of HVOF sprayed WC-10Co coatings.

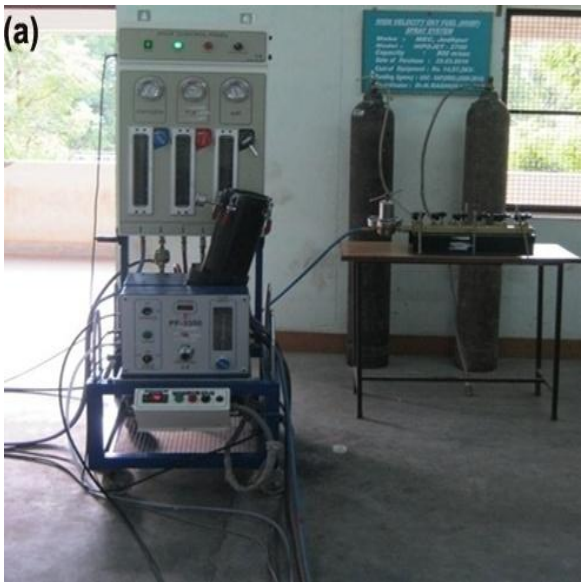

HVOF spraying facility

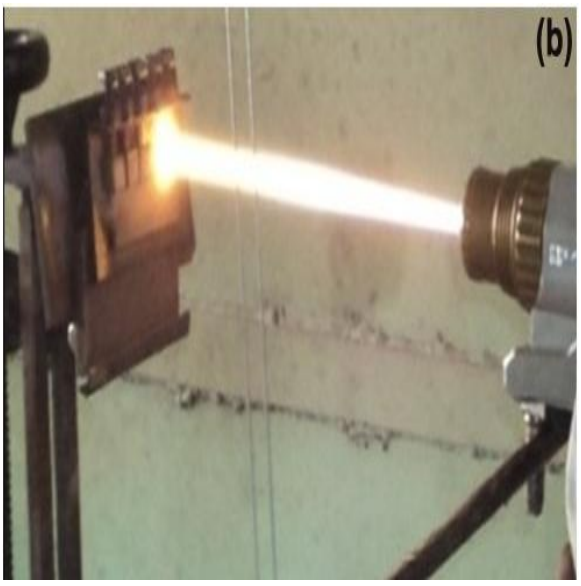

Coating deposition

July – August 2020
ISSN: 0193-4120 Page No. 36 - 55

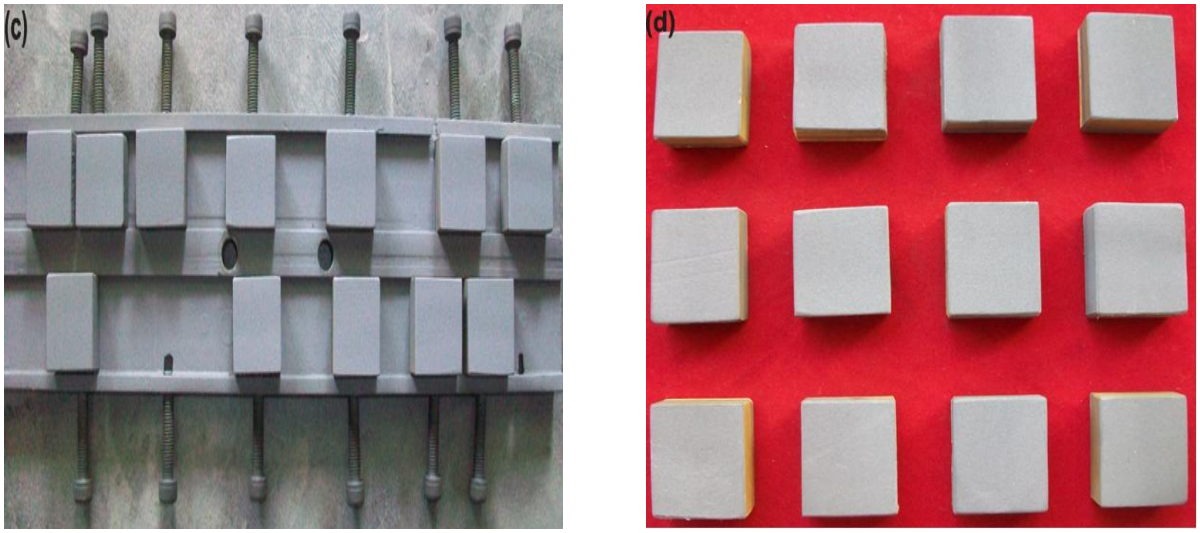

Fig.(b&c) Photographs of WC-10Co coated specimens

Fig.1 Experimental details.

2.1 Coating characterisation

Scanning electron microscopy (Make: JEOL, Japan; Model: 6410-LV) was performed to study the microstructural characterisation and surface morphologies of the powders and coatings. Figure 2(a-b) illustrate the SEM micrograph of the as received powder with spherical morphology with a grain size range of – 45 to +15 µm. The narrow particle size distribution and spherical shaped particles enhance larger melting efficiency and better flow ability. The cross sectional SEM images of coatings are shown in Fig. 2(c–d), accordingly. It can be seen that the very thick coating and has a better adhesion with the substrate. This implies that the coating is tightly attached to the substrate owing to the greater velocity of HVOF thermal spraying. Generally, the optimized settings of HVOF spray process yielded the lowest coating porosity level. This is for the reason higher impact velocity of the coating particles allows high density and cohesive strength of individual splats. The porosity analysis was performed according to the ASTM B 276 [16], on the metallographically prepared cross sections of the coating through optical microscope (Make: Meiji; Japan, Model: MIL-7100) attached with an image analysing software (Metal vision version.6). In this investigation, the photographs recorded under 1000 x magnification via optical spectroscopy were selected for porosity evaluation to show the characteristics of images including the open pores and network of cracks standard. At first, a 400 µm square region was chosen on the polished coating cross section and the micrograph was examined. The same method was done again at five random locations to determine the average percentage of porosity level. The microhardness tester (Make: Shimadzu; Japan. Model: HMV-2T) with a load of 2.94 N and hold time 15s was analyzed the microhardness of coatings. Hardness values were calculated at 10 various spots on the polished cross sectional area of the coating. According to the indention cracking method the fracture toughness of the coated samples were assessed using the HV-5 Vickers hardness tester under a test load 49 N and hold time 15 s. And the average values of 20 experiments were selected as the effective fracture toughness values. The images collected through image analysis and hardness measurements were seen in Figures 3&4. As per the ASTMC-633-01 standard, the coating bonding strength was [17] carried out. By using the E7 glue, the coated specimens were bonded with 35CrMo steel. The measurement was performed on a universal tensile test apparatus after

July – August 2020
ISSN: 0193-4120 Page No. 36 - 55

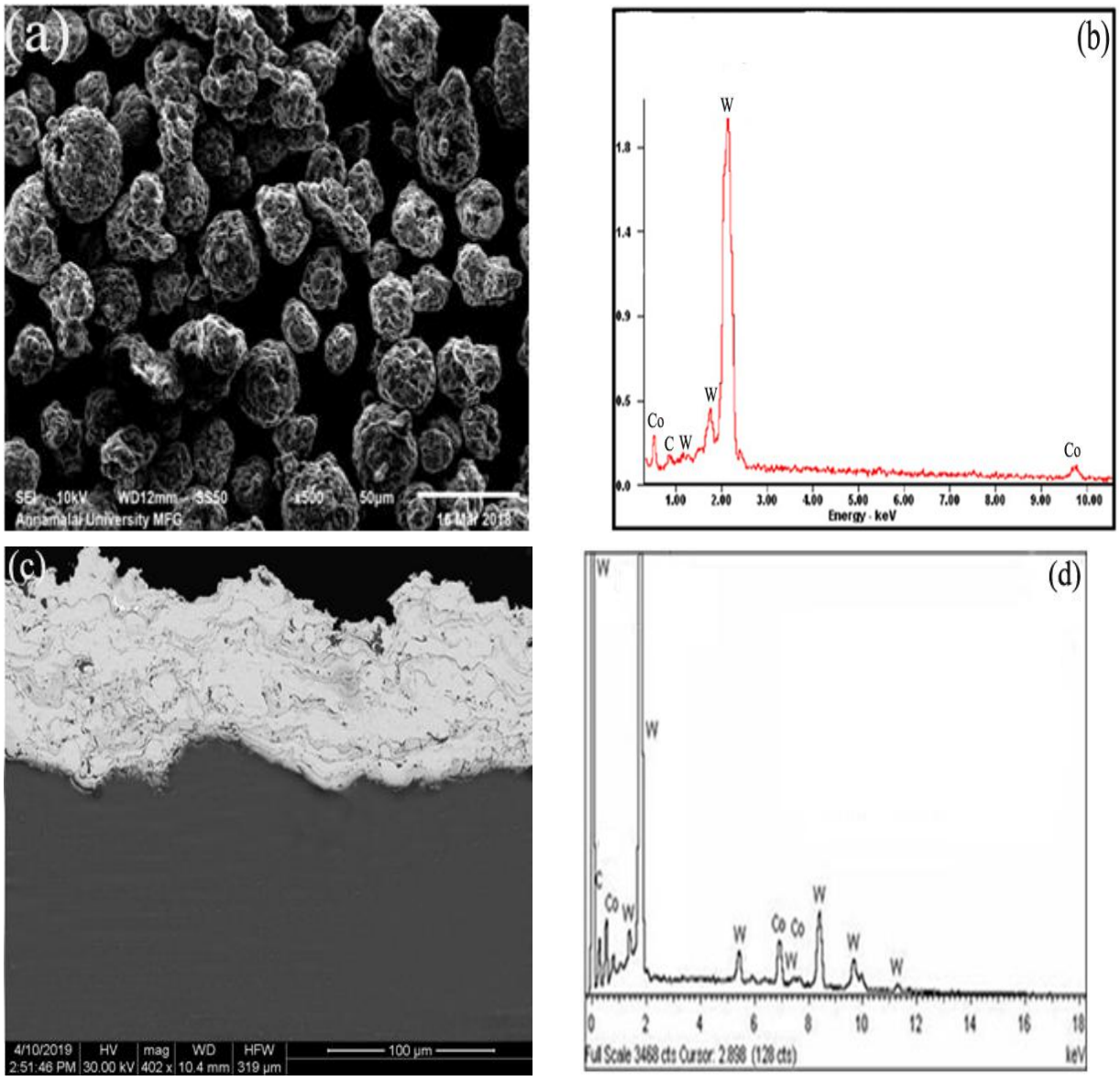

Fig.2 SEM images of WC-10Co powders (a&b) and sprayed coating surfaces (c&d)

July – August 2020
ISSN: 0193-4120 Page No. 36 - 55

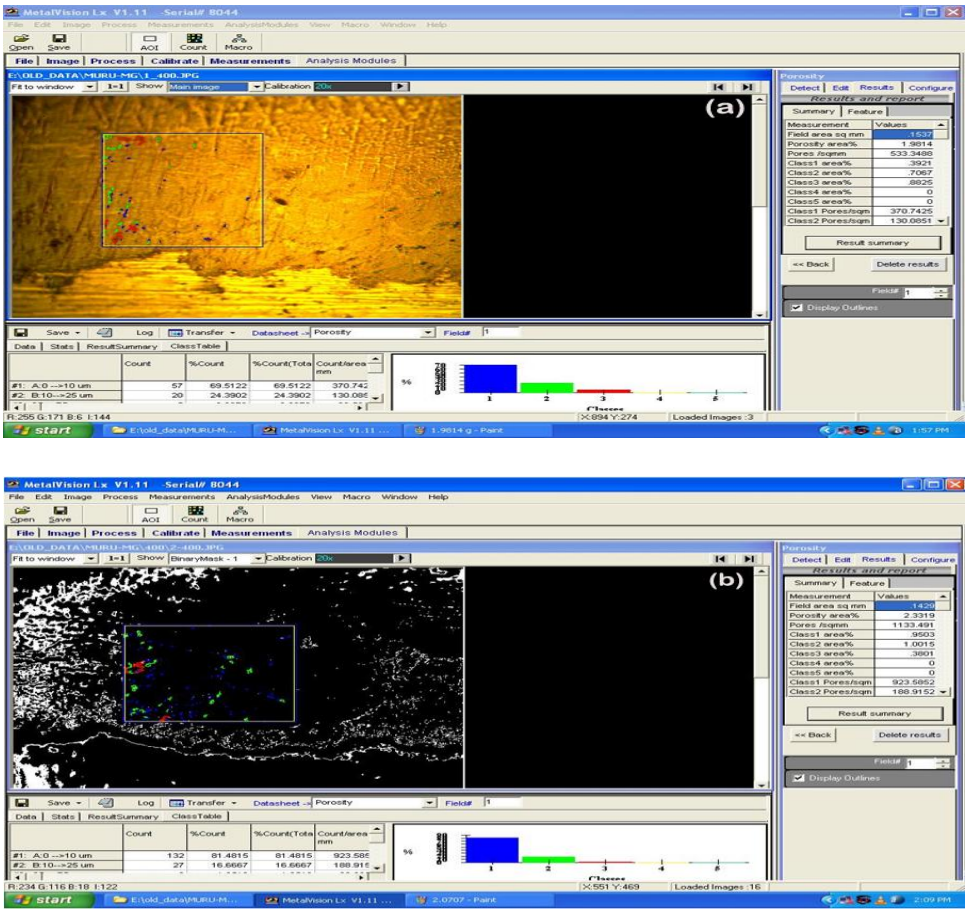

Fig. 3 Steps involved in image analysis; (a) Binary image of the selected image; (b) Selection of area to be analyzed (c) Color coded image after porosity analysis.

TEST Engineering & Management

July – August 2020
ISSN: 0193-4120 Page No. 36 - 55

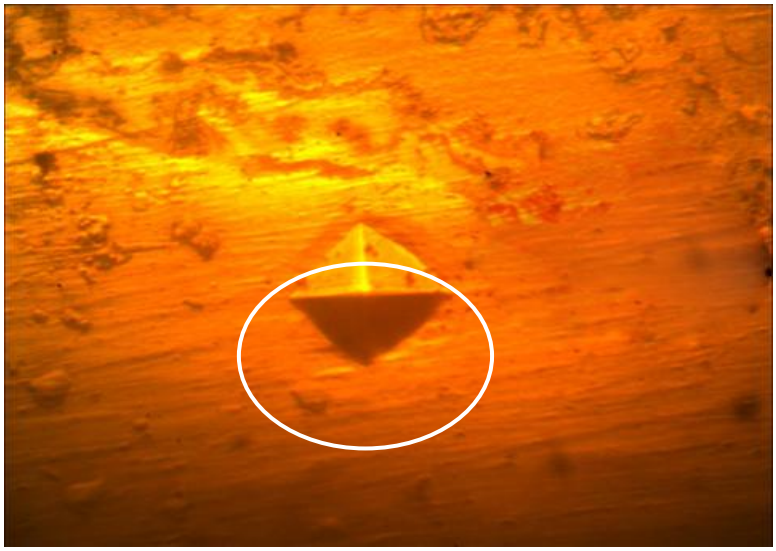

Fig. 4 Indentation image of coating produced under optimum condition

solidification (Make: FIE Blue Star; India. Model: UNITEK-94100). The crosshead speed of the apparatus was 1 mm min−1. The average of three experimental measurements were evaluated to measure the bonding strength of each coating.

2.2 Slurry erosion testing

The influence of angle impingement, rotational speed, impact angle and exposure time on the erosion behaviour of uncoated and coated specimens were measured using slurry erosion tester (Model: TR- 411, Make: DUCOM, India). The experiments were performed to estimate the mass loss of the specimen. The mass loss was determined from weighing the specimens before and after the slurry erosion process (Fig. 5). Slurry erosion experiment was performed on 35CrMo steel specimens of size 25.4 × 76.2 × 5 mm. Prior to the experiments, specimens were polished and ultrasonically cleaned using a precision weighing machine. These specimens having a standard size are fixed onto the disc with the support of clamps at the desired radial distance. The disc along with the specimen is immersed into the slurry contained in the container. The motor is

Slurry jet erosion tester(full view)

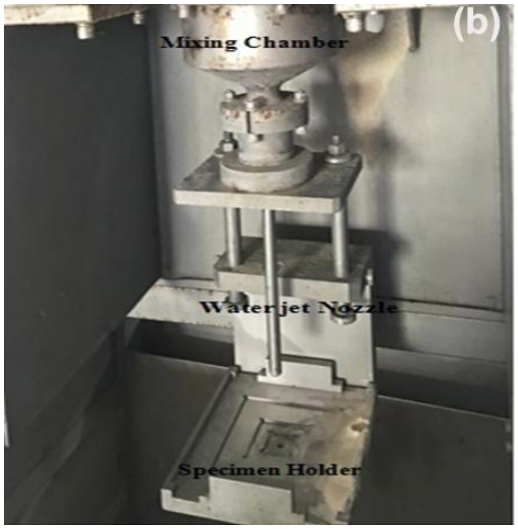

Slurry jet erosion test set up (closer view)

July – August 2020
ISSN: 0193-4120 Page No. 36 - 55

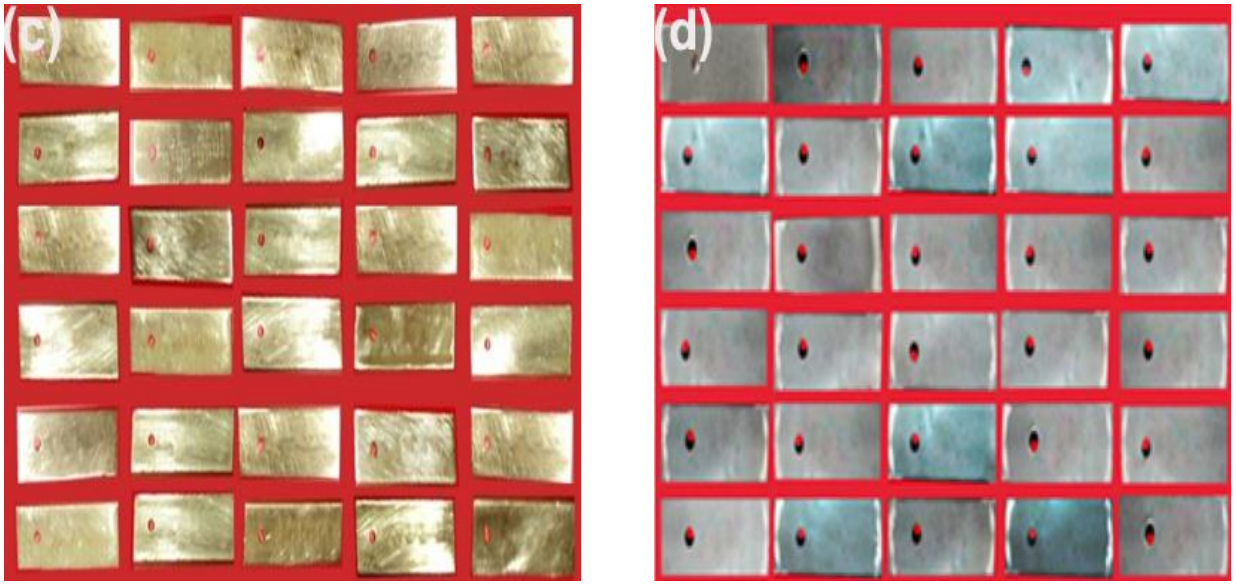

Uncoated specimens **Coated specimens**

Eroded specimen after test

Fig. 5 Specimens for slurry erosion testing

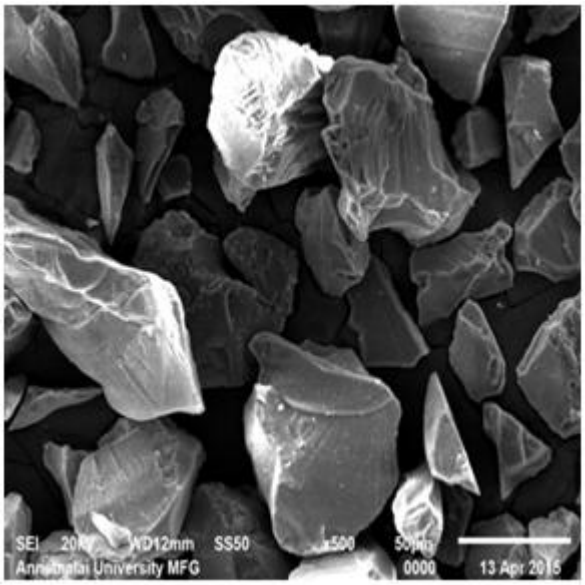

Fig.6 SEM micrograph of erodent particles

July – August 2020
ISSN: 0193-4120 Page No. 36 - 55

commenced, and the specimens are rotated at the desired speed for a given period. After the experiment is performed the specimens were removed, cleaned and weighed. The mass loss is measured with respect to different experimental parameters by the rate of mass loss. Figure 5 (c-d) discloses the photograph of the specimens before and after the erosion experiments. The Quartz sand of 50 μm sizes was used as an erodent in the water jet erosion and slurry erosion experiments and its SEM micrograph is shown in Fig. 6.

2.3 Choosing the ranges of erosion test variables

According to the publications [10-15] and the recent study conducted in our laboratory [18], the primary process inputs that have a greater effect on the slurry erosion behaviour of coatings are selected. They are rotational speed, angle of impingement, slurry concentration and time. Trial research was performed to select the feasible working limits of slurry erosion variables.

2.4 Constructing experimental design model

After considering the possible ranges of the erosion test apparatus as stated under the erosion parameters and their ranges were selected, so that erosive wear study could be carried out without any problem. To minimize the time and cost, statistically designed experiments were used to examine the effect of the slurry erosion parameters on the mass loss. The considered factors with their levels and mass loss for the substrate and as coated specimen is displayed in Tables 2 and 3.

In this study, the experiments were performed in a random structure to avoid systematic failures infiltrating the system. At each experimental condition three experiments had been carried out to confirm the accuracy of the findings.

3. Predictive mathematical model for erosion rate

A response surface model building method was utilized in this investigation, to predict mass loss in terms of rotational speed, impact angle, slurry composition and time. In order to determine responses depend on experimentally determined values, an empirical quadratic relationship was established to compare experimental factors and erosion rate. The responses are function of impact angle (A), rotational speed (S), time (T) and slurry composition (F) and it could be stated as

Responses = f (T, S, A, and F)……..(1)

The final empirical relationships to measure the responses are

Mass loss of uncoated 35CrMo steel substrate = {0.140 + 0.049 (T) + 0.025 (S) + 0.022 (A) - 1.19E-2 (D) – 4.31 E-04 (T)(S) + 9.4E-5 (T)(A) + 6.94E-4 (T)(F) - 1.14E-3 (S) (A) - 1.94E-3(S)(F) - 1.22E-3 (A) (F) + 1.64E-3 (T2) + 1.19E-3(S2) + 1.61E-3(A2) - 1.23E-4 (F2)}……. (2)

Mass loss of WC-10Co coating = {0.11 + 0.04(T) + 1.62E-2 (S) + 1.39E-2 (A) - 7.84E-3 (F) - 3.10E-4 (T) (S) + 3.12E-05(T)(A) + 4.19E-4 (T)(F) - 7.20E-4 (S)(A) - 1.26E-3 (S)(F) - 7.70E-4 (A)(F) + 1.00E-3 (T2) + 7.03E-4 (S2) + 9.66E-4 (A2) - 1.60E-4 (F2)} ……. (3)

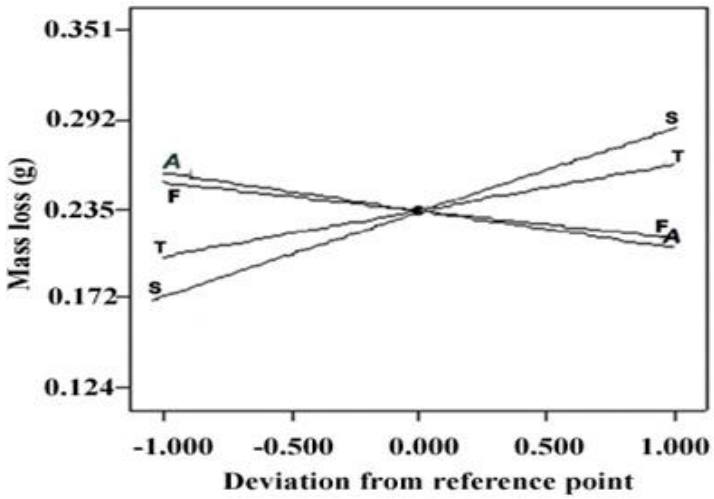

(a) Uncoated 35CrMo steel

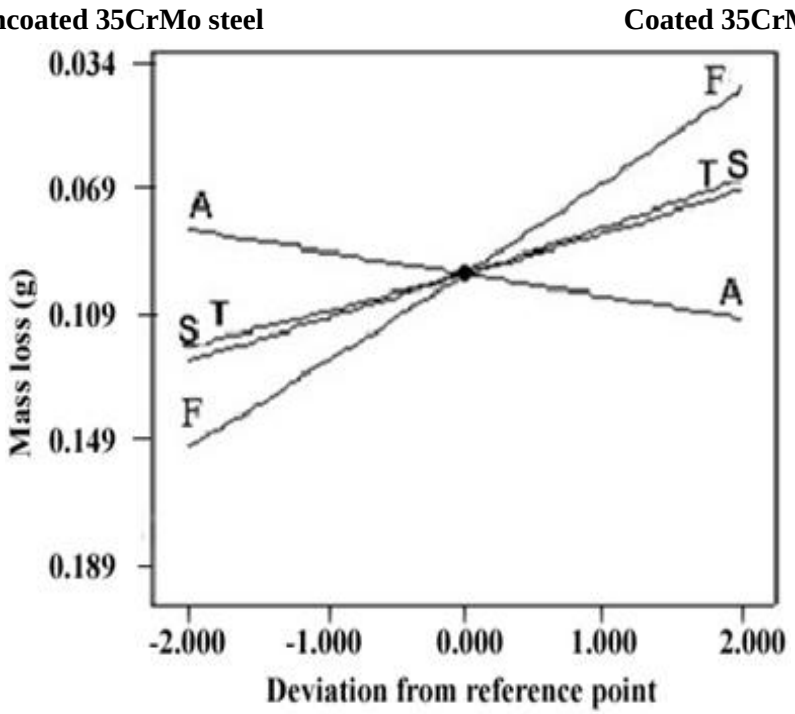

(b) Coated 35CrMo steel

Fig. 7 The perturbation of the effect of factors on the slurry erosion rate

3.1 ANOVA analysis and model fitting

In this research, the adequacy of the established empirical relationships was examined using analysis of variance (ANOVA) method. Tables 4 and 5 reveals the ANOVA study findings of the mass loss of uncoated and as coated samples. The literature [19] provides the procedure for interpreting the ANOVA data.

It was found from tables 4 and 5 that the predominant parameters ('F' value assessment) which have direct influence on the responses as per the order of rotational speed, impact angle, time and slurry composition respectively. Collectively, those findings show the outstanding potential of the regression model. The established empirical relationships could be used efficiently to estimate the responses through replacing the values of experimental parameters in coded format.

4 Results and discussion

4.1 Influence of rotational speed on mass loss

Figure 7 illustrates that the rotational speed is directly proportional relationship with the erosion rate. It is commonly known that Erosion = K × (velocity) ^{n}, where constant 'K' focuses on particle size and impact angle and 'n' is the velocity exponent. The velocity of slurry particles over the contact surfaces of the samples is not uniform in the slurry erosion experiments. The maximum rotational speed appears at the initial contact surface area of the flowing fluid and gradually falls as it reaches the remaining edges. Therefore, given the power law relationship amidst the mass loss and rotational speed, a slight reduction in rotational speed would arise in an amplified decrease of the slurry erosion rate.

The kinetic energy moved to the particle is reduced as the rotational speed is low. The lower the kinetic energy, diminish the opportunity of a good outcome (the erosion reduces) through single impact. Furthermore, in these conditions, at low velocities, the particle flow divergence reduces,

July – August 2020
ISSN: 0193-4120 Page No. 36 - 55

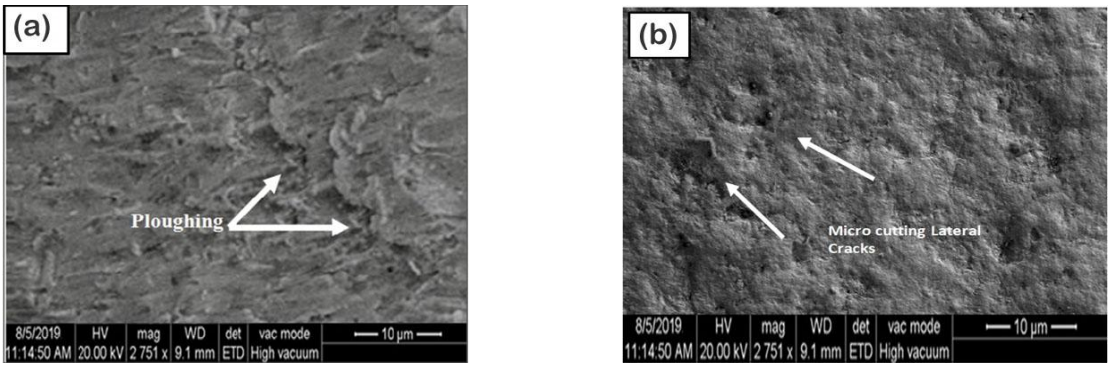

Rotational Speed: 500 m/s, Impact angle: 60°, Time 90 min and Slurry Composition: 300 g/cc

Rotational Speed: 1000 m/s, Impact angle: 60°, Time 90 min and Slurry Composition: 300 g/cc

Rotational Speed: 1500 m/s, Impact angle: 60°, Time 90 min and Slurry Composition: 300 g/cc

Fig. 8 SEM images of eroded uncoated and coated 35CrMo steel at various rotational speeds.

these slurry particles impinge on the surface with low kinetic energies, or at adverse incidence angles, or have many of their translational kinetic energy changed into rotational kinetic energy (particle rotation). Therefore the extraction of material should be minimal of both the substrate and coatings. Microcutting occurs in 35CrMo steel as shown in Fig. 8. Smaller amount of lateral cracks are produced in the lamellae of the coated specimens (Fig. 8 b), when the energy of impact is reduced.

Lateral cracks were not uniform for uncoated and coated samples at the modust energy as could be inferred from Fig.8c&d. If the rotational speed is slightly higher, finally the particles are cannot commence cracking and it will only distort the coatings. On account of the substrate, the lower momentum of the

July – August 2020
ISSN: 0193-4120 Page No. 36 - 55

particle implies that it will continue to rotate on the target surface [20]. As a result, surface damage and small lips can be found in Fig. 8 (a, c).

At high rotational speed conditions, the increase of slurry mass loss of 35CrMo steel might be attributed to the enhanced mechanical distortion because of erosion. Moreover, a greater hardness of the WC-10Co than that of 35CrMo steel may greatly contribute to the higher slurry erosion resistance at high flow velocities [21]. Slurry mass loss occurs when the initial rotational speed of the slurry particle is increased explicitly. This implies that the slurry mass loss is linearly proportional to the velocity square or to the kinetic energy of the suspended particle. It is well known that under the higher rotational speed impact, larger area is removed. The particle enters the surface of the material and ploughs with eliminating the material surface was observed as the shear strain surpasses the elastic strain range of the specified material [22]. As seen in Fig. 8(e) one can expect that the shear force introduced through the suspended particle would improve as a consequence of an enhancing contact velocity of the flowing particle. Thus develop lateral cracks in the coatings as shown in Fig. 8 (e).

4.2 Influence of impact angle on mass loss

Figure 9 presents the influence of impact angle on the mass loss of the substrate and coatings. The worn surfaces of the 35CrMo steel and carbide coatings eroded at an angle of impact of 30° are exhibited in Figures 9a&b. This is demonstrates that the significant plastic shear deformity caused through the sliding behavior of erodent particles. At low the impact particles there was an indication of different actions such as rubbing, extrusion, ploughing, and cutting. There's also evidence of brittle cracking, which definitely leads to material deterioration. Through the micrograph, could see that plastic shearing and rub bands that have been formed because the erodent particles that rubbed the surface during erosion. The micrographs show an erosion pit which was developed through cracking. The contact of target region with erodent particles contributed primarily to ploughing at the impact angle of 60o. From fig.9c&d, it can be found that very scanty to brittle cracking, the erosion at this angle of impact is moderate.

At lower impact angles the highly deformed material developed into “chips” or crater “lips” generated close to normal incidence angles [23, 24]. The erodent particle would have the trend to slide above the surface but as it slides, it will lip the material under moderate angles, as noticed in Fig. 9 c. The consequent particle sliding will eliminate the material from the surface, at low impact angle certain area of the volume swept out could easily be damaged and removed in a ploughing activity. During the sliding the erodent particles were touch for long time on the surface, as a result high wear rate was attained. Because of the various impingement angles of the sand particles the eroded scars have varying lengths and shapes (Figure. 9d). This mode is designated as the cutting mode cracks and lips are illustrated in Fig. 9 e.

As can be observed in Fig. 9 (f), the maximum mass loss calculated under impact of the water slurry lies at angles between 60° and 90° for as sprayed coatings. In the studies of erosion behaviour on tungsten by tap-water slurry, it has also shown that the maximum mass loss occurs at angles between 30° and 60°. The fatigue cracking and brittle breaking are the key reasons for the loss of surface materials for the brittle materials, with the largest erosion occuring at higher impact angle.

For 35CrMo steel, the resistance to erosion decreases with the reduced angle of impact and the maximum erosion occurs at 600, with typical ductile erosion behaviour. It is remarkably found that the mass loss of coatings at all impact angles is much lower than that of uncoated specimens. The mass loss attains a maximum value for as coated samples under the 90° impact angle.

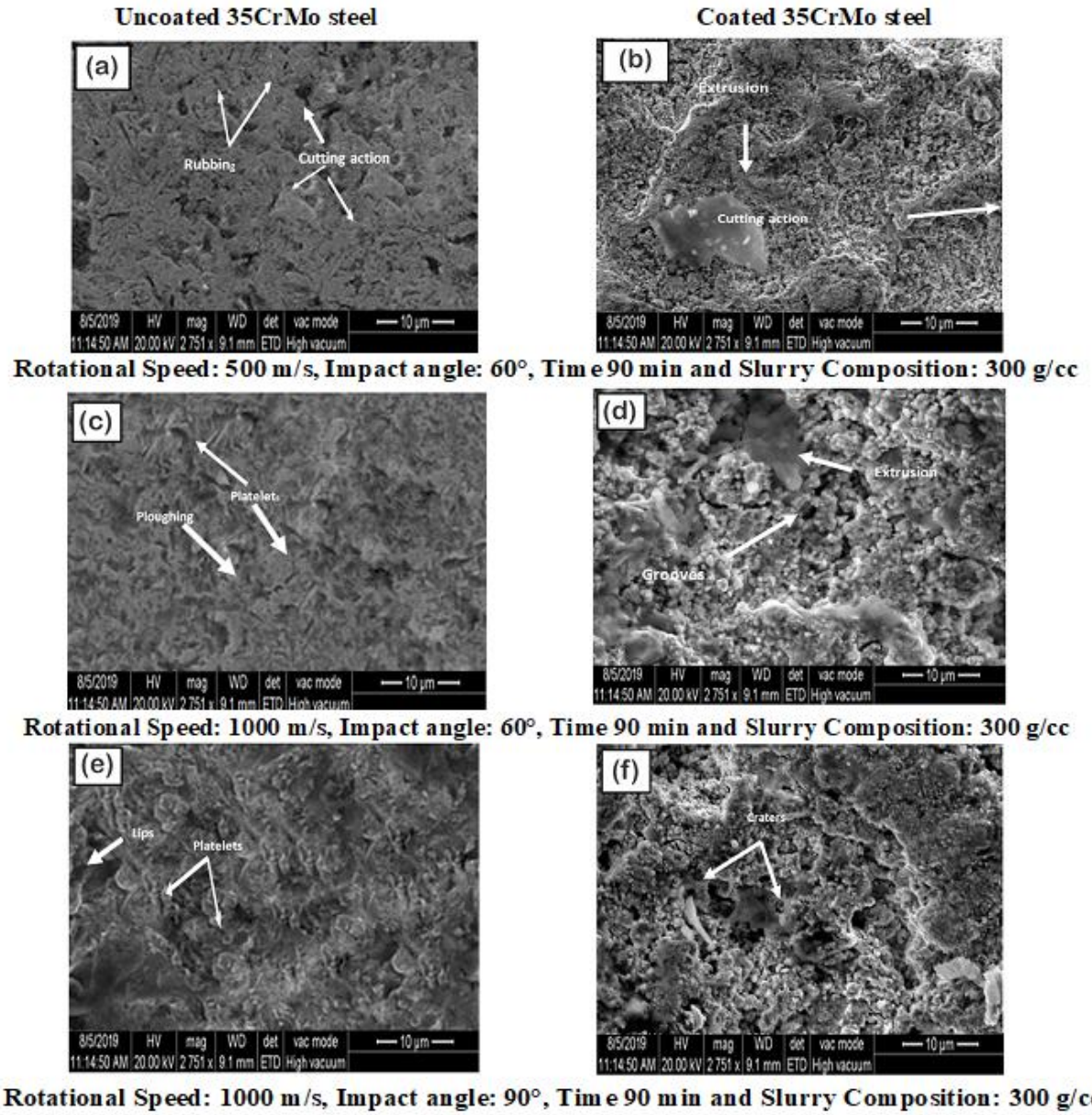

Fig. 9 SEM image of eroded specimens of uncoated and coated 35CrMo steel at various impact angle

4.3 Influence of slurry composition on mass loss

Fig. 10 demonstrates the influence of slurry composition on the rate of erosion of uncoated and coated samples. Erosion rates are observed to raise linearly with increasing slurry composition and reduces with an increase in the angle of impingement. Moreover, the increase in particles in the slurry creates an effect on the crater shape indicates the effect of particles influences on wear rate. SEM micrographs of eroded specimen displays microcutting, plouging and plattte-type failures because of the interaction of slurry particles with the coated surface as seen in Figure 10.

July – August 2020
ISSN: 0193-4120 Page No. 36 - 55

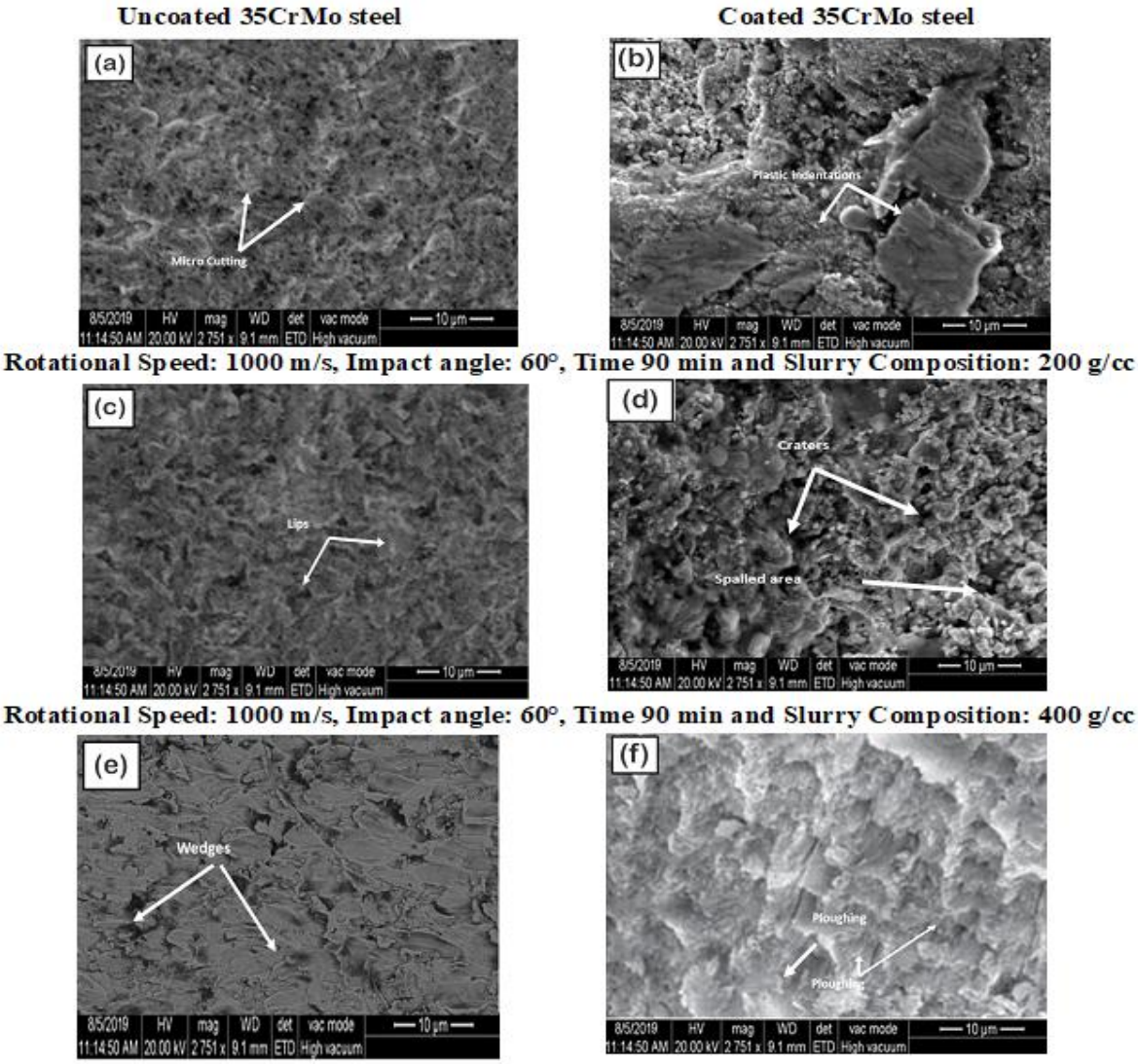

Fig. 10 SEM image of eroded specimens of uncoated and coated 35CrMo steel at various slurry composition

The higher incident energy (impact energy) was observed at low erodent feed rate (i.e. if no-interference effects were appear). As the erodent discharge is decreased at impact, the quantity of erosion loss per unit abrasive mass that hits the target increasing. When the slurry composition is lower, the mean free way of the erodent particles is very lengthy and therefore the probability of collision between both the incident particles and the rebounding particles is extremely low. There is an enhanced circumstance of erosion destruction as the concentration of the particles decreases and the conveying velocity increases [25, 26].

The SEM images (Fig. 10 a, c and e) taken at the top surface of eroded specimens reveals that the uncoated 35CrMo steel had dough marks lateral cracks, microcutting and wedge formation. WC-10Co coatings experienced cracking, splat ejections and lamelle spallation as shown in Fig. 10 b, d and f). From the study of solid particle erosion, it is inferred that at the maximum particle concentrations the mass loss is lower relative to low flux conditions. It can probably be

July – August 2020
ISSN: 0193-4120 Page No. 36 - 55

demonstrated through a realization that maximum numbers of interparticulate and particle - wall collisions will appear at a larger particle concentration.

The effect of the collisions is to accelerate the particles, because some of their kinetic energy is wasted in any collision. Both the substrate and coatings undergo material loss at all the erodent discharge levels. Higher level that proves material removal from the target surface. When the slurry concentration erodent discharge value is higher, hydrodynamic particle interactions arise in the pot arid becomes more prominent as the erodent discharge raises further.
Because as the flux rises, the probability of collision between particles increases dramatically and thus the mass loss will be predicted to reduce. From the fig.10, it is concluded that erosion loss decreases by increasing the rate of erodent discharge. From the slurry erosion, it is evident that the rate of erosion is low compared to low flux conditions at the highest particle concentrations. Nevertheless, mass loss is minimized but the surface damage is increased.

4.3 Influence of time on mass loss

At short time exposure, the rebounding mass loss of more impacting particles from the target surface at higher impact velocity is high compared to the same at least impact velocity. However as the particles were under constant movement owing to steady flow, it is expected that entire kinetic energy of the particles could have not passed to the target surface. Therefore, the mass loss is minimum at low rotational speeds and shorter interval. Neverthless, specimens exposed to slurry environment experiences cutting action in metals, indentation scar in coatings. (Fig. 11 a & b). Similar trends were found at intermediate time, which can be presented in Fig.11 c & d. It is evident from the fundamentals that erosion rates increase at high rotational speed with an increase in exposure time. Because the erosion wear happens, owing to the movement/kinetic energy of impacting particles, it is also predicted that mass loss increases for longer time with the rise in the velocity of impacting particles. This may probably be due to the effects of plastic deformation (Fig. 11 (e & f)) on the surface at higher velocities resulting in the exposure area being increased for further impact. Coated specimen reveals spallation and plastic indentations on the surface after the experiments. The higher hardness and low porosity of HVOF sprayed coatings noticed in low mass loss water solutions [27, 28].

6. Conclusions

In this investigation, the influences of solid particle erosion parameters, respectively, angle of impingement, rotational speed, slurry composition and time were investigated using response surface methodology (RSM) and the following conclusions were drawn.

i. Empirical relationships have been developed using RSM to predicting the mass loss of the uncoated and coated samples.
ii. Of the four parameters evaluated, rotational speed was the most significant parameter influencing the mass loss of the coatings followed by angle of impingement, slurry concentration and time.
iii. Uncoated steel experiences higher mass loss when compared with the WC-10Co coated 35CrMo steel at higher rotational speeds. The eroded surface of the steel substrate is severely damaged whereas WC-10Co coatings also experiences mass loss and surface damage is minimum, around 35 % of wear resistance was improved by utilizing WC-10Co coating system over the 35CrMo steel.

Acknowledgements

The authors wish to convey their deepest gratitude to Department of Manufacturing Engineering, Annamalai University for extending facilities to characterize the coatings.

REFERENCES

[1] Qun Wang, Sisi Luo, Shaoyi Wang, et al. Wear, erosion and corrosion resistance of HVOF-sprayed WC and Cr_3C_2 based coatings for electrolytic hard chrome replacement. Int J Refract Met H. 2019; 81: 242-252.

July – August 2020
ISSN: 0193-4120 Page No. 36 - 55

[2] Edward Anand E, & Natarajan S. High temperature erosion behaviour of plasma-sprayed NiCrBSi–graphite coatings. Surf Eng. 2018; 34(10): 783–790.

[3] Gursharan Singh, Sukhinderpal Singh & Jasmaninder Singh Grewal. Erosion wear characterisation of DLC and AlCrN based coated AISI-304/316 steels. Surf Eng. 2019; 35(4): 304–316.

[4] Xiangdong Men, Fenghe Tao, Lin Gan, et al. Erosion behavior of Ni-based coating under high speed hot airflow. Surf Eng. 2019; 35 (8): 1–10.

[5] Wang Q, Tang Z, Cha L. Cavitation and sand slurry erosion resistances of WC-10Co- 4Cr coatings. J Mater Eng Perform. 2015; 24 (6): 2435–2443

[6] Ding X, Ke D, Yuan C Q, et al. Microstructure and cavitation erosion resistance of HVOF deposited WC-Co Coatings with different sized WC. Coatings, 2018; 8 (9): p 307.

[7] Xiao-bin Liu, Jia-jie Kang, Wen Yue, et al. Performance evaluation of HVOF sprayed WC-10Co-4Cr coatings under slurry erosion. Surf Eng. 2019; 35 (9), 816–825

[8] Vibhu sharma, Manpreet kaur and Sanjeev bhandari. Micro and nano ceramic-metal composite coatings by thermal spray process to control slurry erosion in hydroturbine steel: an overview. Eng Res Express. 2019; 1(9): 012001.

[9] Anuj Bansal, Jagtar Singh, Harpreet Singh. Slurry erosion behavior of HVOF sprayed WC-10Co-4Cr coated SS 316 steel with and without PTFE modification. J Therm Spray Tech. 2019; 28(19): 1448–1465.

[10] Xiao-bin Liu, Jia-jie Kang, Wen Yue, et al. Performance evaluation of HVOF sprayed WC-10Co-4Cr coatings under slurry erosion. Surf Eng. 2019; 370 (9), 1–11

[11] Matikainena V, Rubio Peregrina S, Ojala N, et al. Erosion wear performance of WC- 10Co4Cr and Cr_3C_2-25NiCr coatings sprayed with high-velocity thermal spray processes. Surf Coat Technol. 2019; 370(1): 196–212

[12] Singh, J, Kumar, S. and Mohapatra, S. Erosion wear performance of Ni-Cr-O and NiCrBSiFe-WC (Co) composite coatings deposited by HVOF technique. Ind Lubr Tribol. 2019; 71 (4): 610-619.

[13] Deepak kumar goyal, Harpreet singh, & Harmesh kumar. Characterization and accelerated erosion testing of WC-Co-Cr- and CoNiCrAlY-coated CA6NM turbine steel. J Therm Spray Tech. 2019; 28, 1363–1378.

[14] Rani M, Perumal G. Roy M, et al. Post processing of Ni-Cr-Al_2O_3 thermal spray coatings through friction stir processing for enhanced erosion–corrosion performance. J Therm Spray Tech. 2019; 28(15): 1466–1477.

[15] Sarbjeet Kaushal, Satnam Singh. Slurry erosion behavior of plasma sprayed coating on turbine steel. Ind Lubr Tribol. 2019; 71 (1), 1-9

[16] ASTM B276-05. Standard test method for apparent porosity in cemented carbides, annual book of ASTM standards, ASTM international, 2010.

[17] ASTM C633 – 01. Standard test method for adhesion or cohesion strength of thermal spray coatings, annual book of ASTM standards, ASTM international, 2008.

[18] Murugan K, Ragupathy A, Balasubramanian V, et al. Developing empirical relationships to predict hardness of WC-Co-Cr HVOF sprayed coating. Procedia Mater Sci. 2014; 5: 918-927

[19] Khuri A I and Cornell J A. Response Surfaces; Design and Analysis, Marcel Dekker Ltd, New York, 1996.

[20] Shahi A S and Pandey S. Modelling of the effects of welding conditions on dilution of stainless steel claddings produced by gas metal arc welding procedures. J Mater Process Technol. 2008; 196(1): 339-344.

[21] Kumar S, Kumar P and Shan H S. Effect of evaporative pattern casting process parameters on the surface roughness of Al-7% Si alloy castings. J Mater Process Technol, 2007; 182(1), 615-623.

[22] Zhao J, Ma A, Ji X, et al. Slurry erosion behavior of AlxCoCrFeNiTi0.5 high-entropy alloy coatings fabricated by laser cladding. Metals. 2018, 8(126), 1–12.

[23] Vinayaka R. Kiragi, Amar Patnaik, et al. Parametric optimization of erosive wear response of TiAlN-coated aluminium alloy using taguchi method. J Mater Eng Perform. 2019; 28(1), 838–851.

[24] Jha A K, Batham R, Ahmed M, et al. Effect of impinging angle and rotating speed on erosion behavior of aluminum. Trans Nonferrous Met Soc China. 2011, 21(1), 32–38

[25] Jianhua zhao, Aibin ma, Xiulinji, Jinghua jiang and Yayun bao. Slurry erosion behavior of AlxCoCrFeNiTi0.5 high entropy alloy coatings fabricated by laser cladding. Metals, 2018; 8(12):1-12.

[26] Naveena B E, Keshavamurthy R, Sekhar N. Slurry erosive wear behaviour of plasma sprayed

July – August 2020
ISSN: 0193-4120 Page No. 36 - 55

fly ash Al_2O_3coatings. Surf Eng. 2017; 33(12): 925–935.

[27] Jianhua zhao, Aibin ma, Xiulinji, Jinghua jiang and Yayun bao. Slurry erosion behavior of AlxCoCrFeNiTi0.5 high entropy alloy coatings fabricated by laser cladding. Metals, 2018; 8(12):1-12.

[28] Naveena B E, Keshavamurthy R, Sekhar N. Slurry erosive wear behaviour of plasma sprayed fly ash Al_2O_3coatings. Surf Eng. 2017; 33(12): 925–935.

Table captions

Table 1 HVOF process variables.
Table 2 Slurry erosion experimental factors and their ranges
Table 3 The design matrix and measured responses.
Table 4 ANOVA experimental findings for uncoated substrate
Table 5 ANOVA experimental findings for coatings

Figure captions

Fig.1 Experimental details.
Fig.2 SEM micrographs of WC-10Co powders (a&b) and sprayed coating surfaces (c&d)
Fig.3 Steps involved in image analysis; (a) Binary image of the selected image; (b) Selection of area to be analyzed (c) Color coded image after porosity analysis.
Fig.4 Indentation image of coating produced under optimum condition
Fig.5 Specimens for slurry erosion testing
Fig.6 SEM micrograph of erodent particles
Fig.7 Perturbation plots
Fig.8 SEM images of eroded uncoated and coated 35CrMo steel at various rotational speeds
Fig.9 SEM image of eroded specimens of uncoated and coated 35CrMo steel at various impact angles
Fig.10 SEM image of eroded specimens of uncoated and coated 35CrMo steel at various slurry composition
Fig.11 SEM image of eroded coated and uncoated 35CrMo steel at various exposure time

TABLES

Table 1 HVOF process variables

Process parameters	Values
Oxygen flow rate	253 lpm
LPG flowrate,	61 lpm,
Powder feed rate	35 g/min
Spray distance	227mm

Table 2 Slurry erosion experimental factors and their ranges

No	Factor	Units	Notation	Levels				
				-2	-1	0	1	2
1	Impact angle	degree	A	30	45	60	75	90
2	Rotational Speed	rpm	S	500	750	1000	1250	1500
3	Time	min	T	30	60	90	120	150
4	Slurry Composition	g/cc	F	200	300	400	500	600

July – August 2020
ISSN: 0193-4120 Page No. 36 - 55

Table 3 The design matrix and measured responses.

Exp. condition	Time (min)	Rotational Speed (rpm)	Impact angle (degree)	Slurry Composition (g/cc)	Mass loss of uncoated steel (g)	Mass loss of coated steel (g)
1	60	750	45	300	0.0580	0.0512
2	120	750	45	300	0.1543	0.1147
3	60	1250	45	300	0.1141	0.0881
4	120	1250	45	300	0.2087	0.1504
5	60	750	75	300	0.1047	0.0819
6	120	750	75	300	0.2014	0.1456
7	60	1250	75	300	0.1562	0.1160
8	120	1250	75	300	0.2512	0.1784
9	60	750	45	500	0.0390	0.0387
10	120	750	45	500	0.1381	0.1040
11	60	1250	45	500	0.0873	0.0706
12	120	1250	45	500	0.1847	0.1346
13	60	750	75	500	0.0809	0.0664
14	120	750	75	500	0.1804	0.1318
15	60	1250	75	500	0.1246	0.0954
16	120	1250	75	500	0.2224	0.1595
17	30	1000	60	400	0.0493	0.0456
18	150	1000	60	400	0.2434	0.1733
19	90	500	60	400	0.0955	0.0759
20	90	1500	60	400	0.1936	0.1406
21	90	1000	30	400	0.1041	0.0815
22	90	1000	90	400	0.1885	0.1372
23	90	1000	60	200	0.1632	0.1205
24	90	1000	60	600	0.1154	0.0891
25	90	1000	60	400	0.1396	0.1049
26	90	1000	60	400	0.0580	0.0512
27	90	1000	60	400	0.1543	0.1147
28	90	1000	60	400	0.1141	0.0881
29	90	1000	60	400	0.2087	0.1504
30	90	1000	60	400	0.1047	0.0819

July – August 2020
ISSN: 0193-4120 Page No. 36 - 55

Table 4 ANOVA experimental findings for uncoated substrate

Source	Sum of squares	Df	Mean square	F Value	p-value prob > F	
Model	0.08532	14	0.006094	53136.33	< 0.0001	Significant
T-Time	0.056503	1	0.056503	492648.4	< 0.0001	
S-Rotational speed	0.01444	1	0.01444	125905.9	< 0.0001	
A-Impact angle	0.010681	1	0.010681	93126.64	< 0.0001	
F-Slurry composition	0.003425	1	0.003425	29861.63	< 0.0001	
TS	2.98x10-6	1	2.98 x10-6	25.94463	< 0.0001	
TC	1.41 x10-7	1	1.41 x10-7	1.226117	< 0.0046	
TA	7.7 x10-6	1	7.7 x10-6	67.14216	< 0.0001	
SA	2.09 x10-5	1	2.09 x10-5	182.4952	< 0.0001	
SF	6.05 x10-5	1	6.05 x10-5	527.0722	< 0.0001	
AF	2.38 x10-5	1	2.38 x10-5	207.2137	< 0.0001	
T^2	7.37 x10-5	1	7.37 x10-5	642.6219	< 0.0001	
S^2	3.88 x10-5	1	3.88 x10-5	338.2273	< 0.0001	
A^2	7.15 x10-5	1	7.15 x10-5	623.1701	< 0.0001	
F^2	4.17 x10-7	1	4.17 x10-7	3.633659	0.0760	
Residual	1.72 x10-6	15	1.15 x10-7			
Lack of Fit	0	10	0	0	1.0000	not significant
Pure Error	1.72 x10-6	5	3.44 x10-7			
Cor Total	0.085322	29				

Table 5 ANOVA experimental findings for coatings

Source	Sum of Squares	Df	Mean Square	F Value	p-value Prob > F	
Model	0.036961	14	0.00264	7002.918	< 0.0001	Significant
T-Time	0.024455	1	0.024455	64866.18	< 0.0001	
S-Rotational speed	0.006276	1	0.006276	16646.95	< 0.0001	
A-Impact angle	0.004651	1	0.004651	12336.74	< 0.0001	
F-Slurry composition	0.001474	1	0.001474	3910.434	< 0.0001	
TA	1.5x10-6	1	1.5 x10-6	3.980438	<0.0045	
TB	1.56x10-8	1	1.56 x10-8	0.041446	<0.0014	
TC	2.81 x10-6	1	2.81 x10-6	7.441976	<0.0006	
SA	8.27 x10-6	1	8.27 x10-6	21.92473	<0.0003	
SF	2.53 x10-5	1	2.53 x10-5	66.97779	< 0.0001	
AF	9.46 x10-6	1	9.46 x10-6	25.08123	<0.0002	

July – August 2020
ISSN: 0193-4120 Page No. 36 - 55

T^2	2.76 x10-5	1	2.76 x10-5	73.21026	< 0.0001	
S^2	1.36 x10-5	1	1.36 x10-5	35.96888	< 0.0001	
A^2	2.56 x10-5	1	2.56 x10-5	67.83891	< 0.0001	
F^2	6.97 x10-7	1	6.97 x10-7	1.848001	0.1941	
Residual	5.66 x10-6	15	3.77 x10-7			
Lack of Fit	0	10	0	0	1.0000	not significant
Pure Error	5.66 x10-6	5	1.13 x10-6			
Cor Total	0.036967	29	3.77 x10-7			